Cover page

מכון ויצמן למדע
WEIZMANN INSTITUTE OF SCIENCE
LIBRARY

Femtosecond laser processing of ceria-based micro actuators

Mishuk, Eran; Shklovsky, Jenny; Berg, Yuval

https://weizmann.esploro.exlibrisgroup.com/discovery/delivery/972WIS_INST:ResearchRepository/1276776400003596?l#1376776390003596

Mishuk, Shklovsky, J., Berg, Y., Vengerovsky, N., Paul, T., Kotler, Z., Tsur, Y., Shacham-Diamand, Y., Krylov, S., & Lubomirsky, I. (2019). Femtosecond laser processing of ceria-based micro actuators. Microelectronic Engineering, 217. https://doi.org/10.1016/j.mee.2019.111126
Document Version: Accepted

Published Version: https://doi.org/10.1016/j.mee.2019.111126

https://weizmann.alma.exlibrisgroup.com/discovery/search?vid=972WIS_INST:ResearchRepository
library@weizmann.ac.il
CC BY-NC-ND V4.0
Free to read
downloaded on 2023/01/03 18:53:09 +0200

Please do not remove this page

Femtosecond Laser Processing of Ceria-Based Micro Actuators

Eran Mishuk*,[1], Jenny Shklovsky*,[2], Yuval Berg*,[3,5], Niv Vengerovsky[3], Tanmoy Paul[4], Zvi Kotler[5], Yoed Tsur[4], Yosi Shacham-Diamand[3], Slava Krylov[2], Igor Lubomirsky[1]

1 Department of Materials and Interfaces, Weizmann Institute of Science, Hertzl st. 234, Rehovot 7610001, Israel

2 Faculty of Engineering, School of Mechanical Engineering, Tel Aviv University, Ramat Aviv, Tel Aviv 69978, Israel

3 Faculty of Engineering, Department of Physical Electronics, Tel Aviv University, Ramat Aviv, Tel Aviv 69978, Israel

4 Department of Chemical Engineering, Technion – Israel Institute of Technology, Haifa 3200003, Israel

5 Additive Manufacturing Group, Orbotech Ltd, Yavne 81101, Israel

*** Contributed equally**

Keywords: MEMS, Actuator, Doped ceria, Femtosecond laser, Micromachining

Abstract

In this paper we present a novel femtosecond laser micro-processing of gadolinium doped cerium oxide (CGO) taking advantage of the unique properties of the ultra-short laser pulse. The process can be extended to other materials which are incompatible with conventional deposition/patterning/etching processes. For example, CGO electrostrictive ceramics is lead-free and non-toxic, compatible with Si-microfabrication and exhibits large electrostriction effect at low frequencies. These qualities make CGO into a promising electroactive material for MEMS applications. However, conventional CGO lithography suffers from low yield due to metal shorts and due to damage during the etch and clean processes. Wet patterning of CGO is very difficult and often results in enhanced leakage or shorts between electrodes. These process compatibility issues can be avoided by using laser patterning. As a proof of concept, a precise patterning of electro-active ceramic $Ce_{0.95}Gd_{0.05}O_{1.975}$ (CGO5) thin films (1.7 μm-thick) by femtosecond laser is demonstrated. The femtosecond laser patterning was used to fabricate double-clamped beam actuators made of CGO5 sandwiched between two metal contacts. The new process is studied and preliminary guide lines are presented. The process design rules are established; for example, a margin between the top contact edges and the CGO layer edges was defined prior to laser ablation to prevent a short-circuiting between top and bottom contacts due to metal ablation. Electro-mechanical testing of the resulting devices demonstrates the long-term mechanical and electrical endurance of 1.2 mm long beams. Using electrical excitation (voltage amplitude of 10 V with a carrier frequency of 10 MHz modulated at 10 Hz), actuation at 10 Hz induced an in-plane strain of 7×10^{-6} without any observable mechanical degradation for more than 800k cycles. The processes presented in this work, therefore, provide a technological framework for integration of CGO into MEMS-devices.

1. Introduction

Integration of functional ceramic (e.g. piezoelectric or electrostrictive materials) into microelectromechanical systems (MEMS) is one of the promising pathways to miniaturized sensor and actuators realization. Similar to electrostatically operated devices, piezoelectric actuators consume low power and can be operated dynamically at high frequencies. In contrast to their electrostatic counterparts, piezoelectric devices can be driven by lower voltages, exert much higher forces and are not prone to undesired (so called, pull-in) instabilities. [1] The widely used piezoceramic material, Lead-Zirconium-Titanium Oxide ($PbZr_{1-X}Ti_xO_3$ or PZT), contains lead, which is toxic [2] and is not allowed by most of the fabrication facilities due the danger of contamination. PZT layers typically show residual stress, which may cause an initial bending of micro-mechanical structures, limiting the applicability of potential device configurations. An intensive research is carried out aimed at exploring new lead-free materials with good overall performance and potential of integration with micrometer to millimeter scale devices.

Recently, it was demonstrated that gadolinium-doped ceria ($Ce_xGd_{1-x}O_{2-x/2}$, CGO) exhibits large electrostriction effect. [3-5] As a new material that comes under consideration for microfabrication use, the question to be raised would be: is it possible to integrate CGO into existing fabrication processes? Or, alternatively, what are the modifications of the common fabrication processes which are necessary in order to integrate CGO into MEMS devices. CGO is stable with respect to the common wet etchants used in silicon foundries. It has good mechanical properties and potentially can be produced at low cost, which is an important factor in its application.

One of the challenges of incorporating CGO in MEMS is the difficulty of patterning CGO without compromising its performance[6]. In the previous work[7], patterned CGO structures were fabricated by lift-off of a sacrificial aluminum layer. However, this process included many steps yielding mediocre yield and requiring very tight process control. A common problem in this approaches was that the contacts corroded upon voltage application, probably because of surface proton conduction induced due to the humidity in the gap between the contacts.[7] In this work we show, that among other advantages, Laser Micro-Machining can resolve this problem.

During the past two decades, ultrafast lasers have been shown to be an attractive option for high quality micromachining. [8-15] Femtosecond (FS) micromachining is a mask free contactless technology, fully adaptable for 2D and 3D shapes on almost all materials. [16-18] Laser-material interaction in FS regimes induces very low thermal damages because the thermal diffusion length during the pulse is very small (< 1 nm). At FS regimes, laser-material interaction has high efficiency allowing multiphotonic absorption with interaction times shorter than the energetic transfer from electrons to the lattice. [19] Additional advantages of using the fs laser for patterning are rapid processing, digital patterning and a high aspect ratio of the resultant structures. Laser processing of ceramic materials was extensively studied before, [12, 20] yet very few studies related to MEMS devices 3D fabrication by laser were published [21-23] and more specifically processing of the silicon substrate was of interest. [24, 25] This paper suggests a promising novel method, based on ultrashort laser fabrication of 3D structures in ceramic materials for MEMS application.

Here we report on the fabrication of functional double-clamped beam actuators made of $Ce_{0.95}Gd_{0.05}O_{1.975}$ (CGO5) using FS laser Physical ablation. The method was found to be suitable for fabricating actuators based on patterned CGO films, where the films remain electrically and mechanically stable after processing and electromechanical testing.

2. Materials and methods

2.1 Fabrication

The fabrication procedure of the double clamped beams of Al/Ti/CGO5/Ti/Al is based on the protocol outlined previously in [7], by which the free-standing CGO membranes were successfully produced. The details of the fabrication process are shown in **Figure 1**. Sequential deposition of Al/Ti/CGO5/Ti/Al layers, with thicknesses shown schematically in **Figure 1**a, was carried out by sputtering (ATC Orion Series Sputtering System, AJA International Inc.) on a silicon substrate (undoped, 275 μm thick, [100] oriented, double-sided polished, University Wafer, Inc.) at room temperature (**Figure 1**b). A base pressure $<5\times10^{-7}$ Torr was reached in the sputtering chamber prior to the deposition. Al and Ti with thicknesses of ≈ 125 nm and ≈ 250 nm, respectively, were deposited in a pure Ar environment (3 and 5 mTorr, respectively) using DC power (200 W and 150 W, respectively). CGO5 with a thickness of ≈ 1.7 μm was deposited from a stoichiometric 3-inch target (>99.9%, Tzamal D-chem LTD.) using 10:1 Ar:O_2 mixture with 100 W RF

power at a pressure of 30 mTorr. Ti (250 nm) and Al (125 nm) layers were deposited on the CGO5 using the same conditions as before. The metallic and the ceramic films were deposited at room temperature in the same sputtering chamber without breaking the vacuum. Next, aluminum layer (≈ 300 nm thick) was deposited on the back side of the silicon substrate to provide a mask. The top Ti/Al layers and the back-side aluminum layer were patterned by photolithography (***Figure 1*c**) with AZ-4562 photoresist and etched in diluted HF (5% v/v) solution. Back-side alignment was carried out to align the top Ti/Al contact with the rectangle openings of the back-side Al layer. To fabricate free-standing membranes, the rectangle openings were produced by etching the silicon in a Deep Reactive Ion Etching (DRIE, STS-ICP) instrument using Bosch process with SF_6 and O_2 gasses for the etching step and C_4F_8 for the passivation step. Back-side aluminum layer served as a mask and as an etch stopping layer for the DRIE process. The 2-inch silicon wafer provided 21 test specimens, each containing five rectangular membranes of different lengths to test the mechanical stability of the structures. The smallest rectangle is 0.5 mm × 0.8 mm and the largest is 0.5 mm×1.5 mm. Finally, a femtosecond laser-based micromachining setup was used to ablate two rectangular pieces of the self-supported structure around the top contact, in order to form the beam shape (**Figure 1**d).

A scanning electron micrograph (SEM) shows the 1.7 μm thick CGO5 film with very good adhesion to the Ti/Al/Si substrate (**Figure 2a**). The 1.7 μm thick CGO and electrode layers were patterned by an ultrafast laser (Amplitude Systems Tangerine HP), with a pulse duration of 270 fs at a wavelength of 343 nm, with a repetition rate of 175 kHz (**Figure 2**b). A fast-galvanometric scanner followed by an F-theta lens (focal length of 100 mm) scanned the linearly-polarized 17 μm diameter Gaussian laser spot on the surface. The pulse energy was set by an internal acousto-optic modulator, used to optimize the process window by a design of experiments (DOE), based on varying energy in the range between 0.1 μJ and 2 μJ, scanning velocity in the range between 10 mm/sec and 200 mm/sec and pattern repetitions from 1 to 5. In order to verify a full clean cut through the layers, three repetitions of the pattern were used at an energy per pulse of ≈ 0.6 μJ (slightly above CGO ablation threshold), corresponding to a fluence of 260 mJ/cm^2. The pulse energy and the pulse repetition rate (PRR) were optimized to have minimal thermal effects, while maximizing the processing rate (throughput). A suction system was engaged during the laser processing, in order to remove particles generated due to ablation of the CGO. No traces of debris were observed.

2.2 Characterization

The shape of the free-standing structures was characterized using optical profilometry (ZETA-20 3D optical profiler) before and after laser ablation. Impedance spectroscopy (model HVB300 with an Alpha-A modular measurement system, Novocontrol Technologies GmbH & Co. KG) was performed between the range of 0.1 Hz to 0.1 MHz with an excitation voltage of 10 V in a two-parallel plate electrode configuration. Modeling of impedance spectra was performed by determining the distribution function of relaxation times (DFRTs) coupled with Impedance Spectroscopy Genetic Programing (ISGP) software. [26-32] The fitting with various well-known peaks such as Gaussian, Lorentzian, hyperbolic-Secant, pseudo delta, etc. is done by a modified genetic algorithm. The best DFRT model is chosen mainly by combination of least discrepancy and lowest number of free parameters. The consistency of DFRT peaks and the discrepancy in assigning the peaks from ISGP is discussed elsewhere. [32]

Cyclic voltammetry (B2912A Precision Source/Measure Unit, Keysight Technology Inc.) was carried out by linearly sweeping the voltage between -10 V and +10 V at different rates. the bias was applied between the high terminal top contact and the low terminal bottom contact.

Electro-mechanical measurements of three beam actuators with 1.2 mm beam length were performed with a feedback controlled atomic force microscope (AFM, NTEGRA with a SMENA head, NT-MDT Spectral Instruments), with the tip positioned at the center of the clamped beam. Vertical displacement signal was recorded with the z-height sensor in response to applied voltage (up to 10 V), which was supplied using a waveform function generator (Rigol DG4062). The tip and the top contact were electrically grounded to prevent electrostatic interactions between the AFM cantilever and the beam. Vertical displacement measurements at the substrate, in proximity to the beams, displayed no response, which verifies that the motion is only due to the movement of the beam and not due to electrostatic force between the surface and the tip.

The electro-thermo-mechanical response of the specimens were tested also at elevated temperatures (up to 100°C) using LDV (Laser Doppler Vibrometer) system installed on a wafer prober (Karl Suss PSM5). The deflection was measured using the displacement mode of LDV (Polytec Gmbth). The LDV is equipped with an OFV-5000 controller and an OFV-534 sensor head with objective lens and integrated CCD video camera, allowing the laser spot positioning and focusing on the beam's middle point. Signals from the

LDV were fed into an oscilloscope (Keysight Technologies, DSOX2004A, 70 MHz). For temperature control, the specimens were mounted on a custom-made holder with built-in thermocouples and heaters controlled via external temperature controller (2416P4, MRC ltd.).

3. Results and discussion

3.1 Geometry and shape

Double clamped beams from at least 10 test specimens (each holding 5 membranes) were obtained from the rectangular buckled membranes by femtosecond laser processing (**Figure 3**a and 3b). Laser ablation yield was very high even for the longest beam in the chip: nine out of the ten beams with the length of 1.2 mm, 0.13 mm wide, were intact after laser ablation (only 1 broke). After DRIE of the cavity in the Si substrate under the electrode-CGO stack layer (prior to the laser ablation) the membranes buckled due to the relaxation of the residual compressive stresses introduced during sputtering and subsequent processing. The membrane's top surface was convex and had a dome-like buckling shape, as shown in the optical 3D-image for the longest membrane in the chip (**Figure 3**c). The large buckled rectangular membranes displayed a midpoint height of $\approx 3\ \mu$m, which was estimated to correspond to an in-plane strain of 0.002% (**Figure 3**d, calculated from the scanned length of post-buckled shape of the membrane with respect to the flat film on the onset of buckling). After formation of the beam's by fs laser processing, the top surface of the self-supported structure became concave (**Figure 3**e). The profile along the long dimension of the beam displayed an almost perfect cosine shape (**Figure 3**f), consistent with the lowest buckling mode of a double clamped beam.

In order to calculate the post-buckling strain as a function of the beam midpoint deflection, we assume that the small deflections $w \ll L$ of the slender beam (illustrated schematically in **Figure 4**) with length L and thickness $d \ll L$, satisfy the Euler-Bernoulli beam assumptions. In addition, ideal clamping conditions are assumed. Then, the midpoint deflection of the beam in the post-buckling state is: [33]

$$w_m = 4r\sqrt{\frac{N}{N_E} - 1} \qquad (1)$$

Here, $r = \sqrt{I/A}$ is the gyration radius of the beam cross section area; $A = bd$ and $I = bd^3/12$ are, respectively, the area and the second moment of area of the uniform cross section and N_E is the Euler buckling force(**Figure 4**). In view of Eq.(1), the axial force N is calculated using the expression:

$$N = N_E\left(1 + \frac{w_m^2}{16r^2}\right) \quad (2)$$

By substituting into Eq.(2) the expression for $N_E = 4\pi^2 EI/L^2$ and $N = \varepsilon \tilde{E} A$, where ε and $\tilde{E} = \frac{E}{(1-\nu^2)}$ are the beam's axial strain and the effective (plane strain) Young's modulus, respectively, and ν is the Poisson's ratio, we obtain the strain in terms of the beam's midpoint deflection:

$$\varepsilon = 4\pi^2\left(\frac{r}{L}\right)^2\left(1 + \frac{w_m^2}{16r^2}\right) = \frac{4\pi^2}{L^2}\left(\frac{d^2}{3} + \frac{w_m^2}{4}\right) \quad (3)$$

Note that in accordance with Eq.(3) the strain is dictated only by the midpoint deflection and the geometry of the beam and is independent on the highly uncertain value of the Young's modulus[34-40]. This allows determination of the initial strain before substrate removal from the buckling height. In accordance with **Figure 3**f, the measured midpoint elevation of the 1.2 mm long buckled beam above its clamped ends was ≈ 9 μm. According to Eq.(3), it corresponds to the in-plane strain of 0.014%. The differences in the in-plane strain in the membrane and in the beam are attributed to the release of the (perpendicular to the beam axis) strain component after the laser ablation and to the conversion of the biaxial strain state into the one-dimensional axial compression.

3.2 Electrical characterization

Each micro machined silicon beam was supplemented with a separate electrical top contact and tested separately. The resistance, measured between the top and the bottom contacts, before and right after laser ablation remained high (> 40 MΩ**)** indicating that no shorts have formed during the process. It should be noted, that laser ablation membranes in the region where the top contacts overlap with the bottom contact caused short-circuited films. To avoid this, the membranes were cut so to leave a margin (a boundary enclose) between the top contact and the laser-ablated region (**Figure 5**a). Therefore, in our devices only 50 - 60% of the beam area is covered by the top contact.

In order to characterize the electrical properties of the double-clamped beam actuators, we performed impedance spectroscopy measurements. The impedance spectra are similar for beams of all sizes, since the area of the top contact (including the substrate supported and the self-supported areas) is approximately the same for all the beams. Nyquist plot of the impedance spectrum appears as an arc - like feature, as shown for the central (longest) beam in the chip (**Figure 5**b). However, the data could not be fitted with a simple parallel RC circuit. Good fitting was obtained with the ISGP analysis coupled to the DFRT approach. According to the DFRT, the data justifies two relaxation peaks (**Figure 5**c) with resistance and capacity of 9.56 GΩ and 1.28 nF (f_1 = 0.013 Hz) and 14.7 MΩ and 1.36 nF (f_2 = 7.9 Hz). Interestingly, these two peaks are similar to earlier report on electronic and ionic contributions of the grain boundaries as obtained for 10 mol% Gd doped ceria. [41, 42] However, the low frequency feature may as well correspond to interfacial polarization near the electrodes. Nevertheless, in the impedance plot both the real and imaginary parts are Kramers-Kronig compatible from 0.1 MHz to 0.01 MHz only (not shown).

Next, cyclic voltammetry (C-V) was performed to study the relative electrical and electrochemical (i.e. if there is any) components and also its electrical stability. At all sweep rates (0.33 – 2 Vs^{-1}), the C-V display loops that are characteristic of charging (**Figure 5**d). The area enclosed by the loops is smaller at lower sweep rates, which is in accordance to the impedance spectroscopy data, and suggests that the relaxation time of this parallel plate capacitor is > 20V/0.33V/s ≈ 1 min. Up to ±10 V, the C-V data does not display any electrochemical effects. This indicates that voltage application does not induce any corrosion of the electrodes and that the structure is electrically stable. This is very different from previous attempts where micro-bridges and micro-cantilevers structures of CGO have failed because of rapid corrosion of the electrodes upon electrical excitation. [7] This time, the use of a dry laser ablation process, and by separating the top and bottom contacts with a CGO margin, have resulted in electrically stable structures.

3.3 Electro-mechanical response

In view of the large resistance at low frequencies, we have measured the actuation performance in response to high frequency excitation voltage, where Joule heating is expected[5, 43]. The change of the

beam's strain, $\Delta\varepsilon$, as a results of electrical excitation, can be derived from Eq.(3) by taking the derivative of the strain with respect to the midpoint deflection according to:

$$\frac{\partial\varepsilon}{\partial w_m} = 4\pi^2 \frac{w_m}{2L^2} \quad \text{or} \quad \Delta\varepsilon \approx \pi^2 \frac{w_m}{2L^2} \Delta w_m \tag{4}$$

This implies that the larger the buckling height, w_m, the smaller is the change in the midpoint buckling in response to heating $\Delta w_m = (\Delta\varepsilon \cdot 2L^2)/(\pi^2 \cdot w_m)$. Therefore, the smaller the initial strain in the beam, the larger is the change in the displacement caused by the same change in temperature. With a carrier wave of 14 MHz at 10 V, modulated by 10 Hz envelope wave, the 1.2 mm beam displayed more than 700 nm vertical displacement amplitude at the center (**Figure 6**a). This corresponds, according to Eq.(4) to $\Delta\varepsilon$ of ≈2.5×10^{-6}. The thermal response time of the beams was measured by switching the high frequency voltage on and off. As shown for the longest beam in the chip (**Figure 6**b), the thermal response time is ≈ 4 msec. Mechanical endurance tests were carried out as well. We have subjected the 1.2 mm beam to long-term thermal actuation at 100 °C. The displacement amplitude of 2.1 μm, which corresponds to $\Delta\varepsilon$ of ≈7.4×10^{-6}, does not decay after 800,000 cycles (**Figure 6**c), which implies that at this value of periodic strain, CGO based double-clamped beam structure is mechanically reliable.

To check whether electrostriction is observable at low frequencies, we applied a square DC pulse of 10 V and monitored the height at the center of the 1.2 mm beam with an AFM. After 5 sec, a vertical displacement of 100 nm was detected (**Figure 6**d). The displacement is very small, probably, because of the parasitic impedance at low frequencies (see impedance data), suggesting that practical applications demand for more reliable contacts. The DC response can be fitted to a two-time constant exponential function with τ_1= 0.35±0.02 sec and τ_2= 6.5±1.1 sec (**Figure 6**d). The complexity of the electro-mechanical response can stem from the superposition of electrochemical processes at the CGO-titanium interface as well as coupling of the electrostriction effect with non-linear elastic constants of the self-supported structure, as described previously in CGO membranes devices. [5, 44] Nevertheless, this relaxation times are very similar to previously reported relaxation time of electrostriction in doped ceria membranes, bulk ceramics and substrate supported films. [3, 7, 45, 46]

4. Conclusion

We have demonstrated applicability of the femtosecond laser processing for fabrication of actuation devices based on CGO as electroactive material. This method was found to be more suitable than other surface micromachining techniques which have failed previously because of rapid corrosion of the electrodes. The dry process used here to pattern the CGO, as opposed to the wet process used previously, sets femtosecond laser processing as a favorable method for fabricating double clamped beam based on CGO and, probably, for processing of other ceramic films. The microfabricated double clamped beams used here demonstrated high mechanical endurance. Electro-mechanical measurement on double clamped beam have reproduced many of the previously observed electro-mechanical properties of self-supported CGO membranes.

Figures

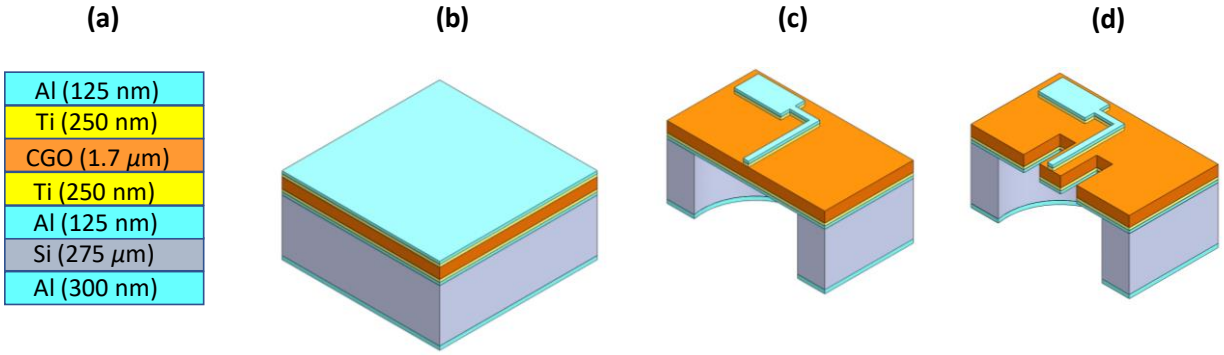

Figure 1. 3-D schematic illustration of the fabrication procedure: (a) the films "stack" scheme indicating their thicknesses, (b) sputter deposition of the corresponding films on silicon substrate, (c) patterning by photolithography, followed by silicon etching with DRIE. (d) femtosecond laser ablation of a membrane pieces around the top contact to form the double clamped beams.

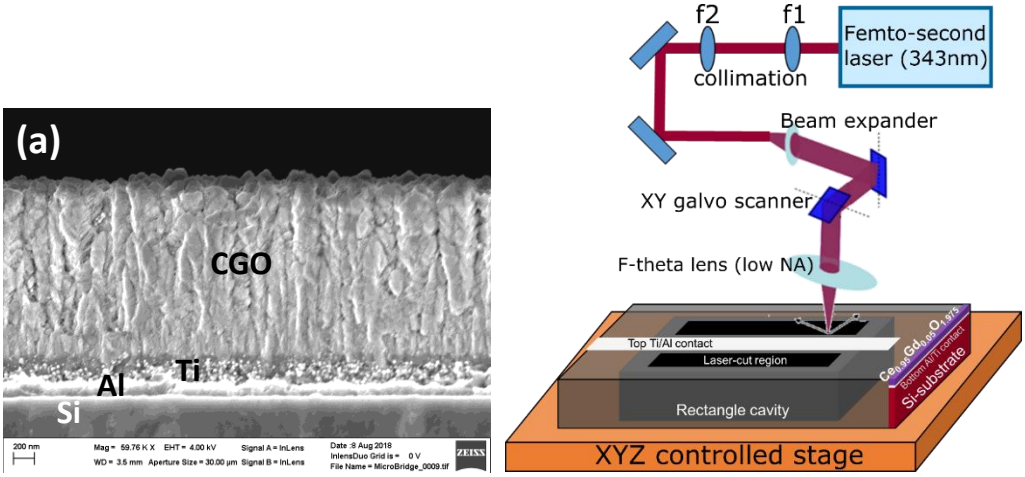

Figure 2. (a) SEM image of the substrate supported CGO5/Ti/Al layered structure 1.7 μm/250 nm/100 nm thick, respectively. (b) schematic representation of the femtosecond laser setup.

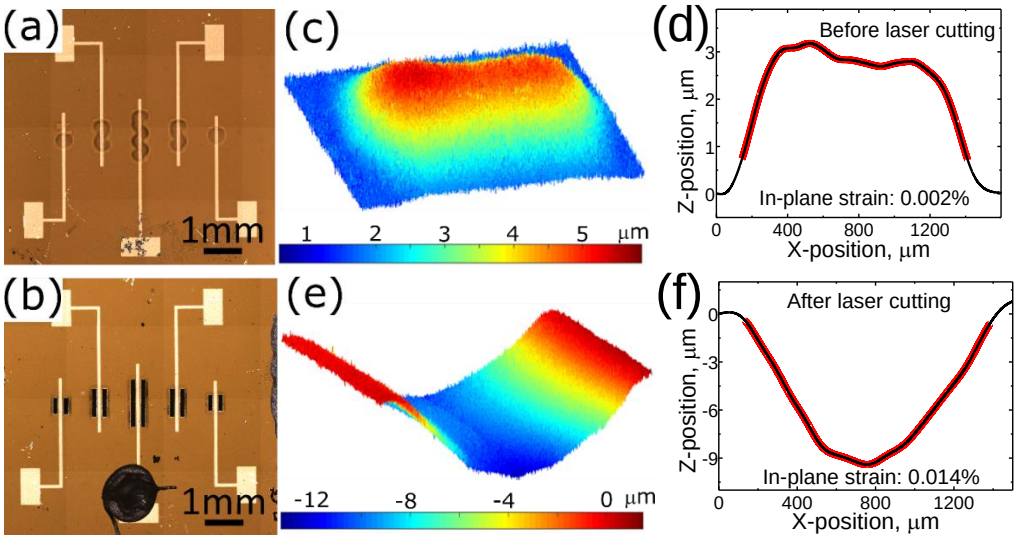

Figure 3. Optical micrograph of a chip (a) prior to laser processing and (b) after laser processing. (c) 3D optical profile image of a 0.5 mm × 1.5 mm rectangular membrane (the longest central device) with the color bar indicative of the Z-height. (d) A line profile measured across the 1.5 mm long membrane in (c). The in-plane strain was measured from the part of the scanned beam marked by the red curve. The clamped ends are leveled at Z=0. (e) 3D optical profile image of the 1.2 mm long beam. (f) Line profile measured across the 1.2 mm long beam.

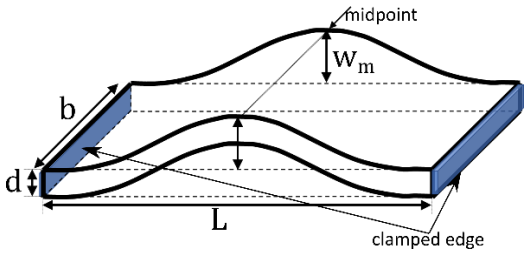

Figure 4. Schematic illustration of the post-buckled state of the double clamed beam with a midpoint deflection w_m, length L, thickness d, and a width b.

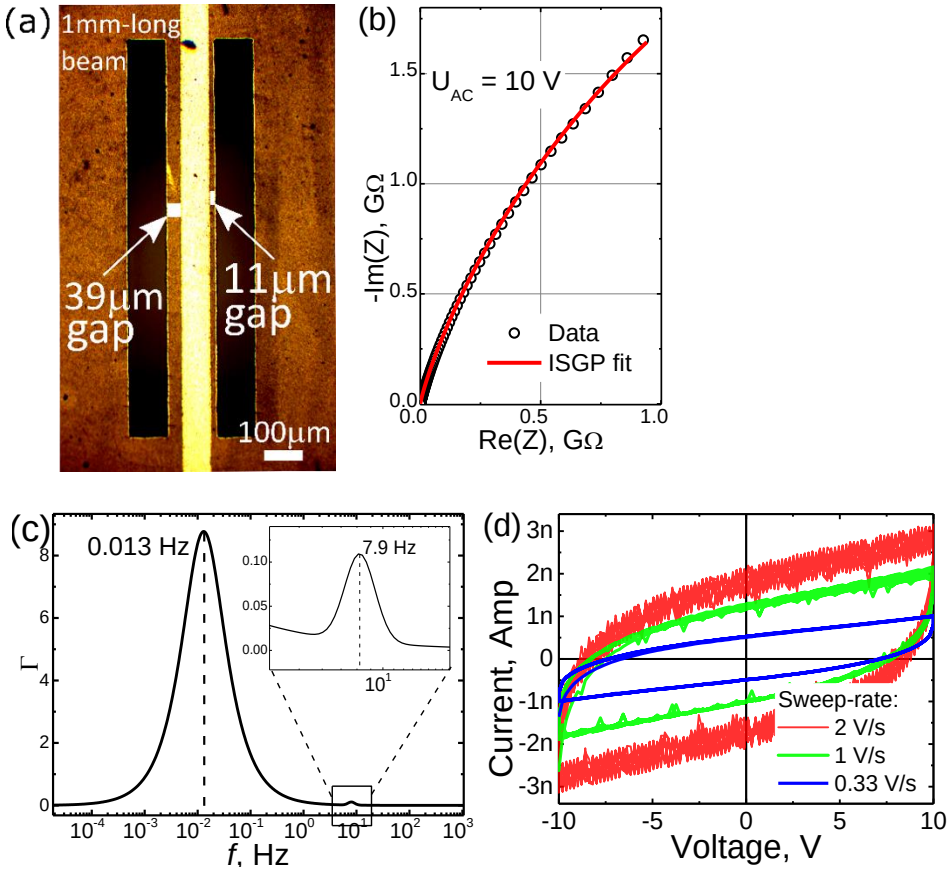

Figure 5. (a) optical micrograph of a 1 mm long double clamped beam. (b) impedance spectroscopy data (square point) for the 1 mm long beam measured between the range of 1 MHz to 1 Hz at excitation voltage of 10 V. Fitting was carried out with the ISGP program (red curve). (c) DFRT analysis of the impedance data in (b) showing two different relaxation frequencies. (d) Cyclic voltammetry data for a 1 mm long beam at different sweep rates.

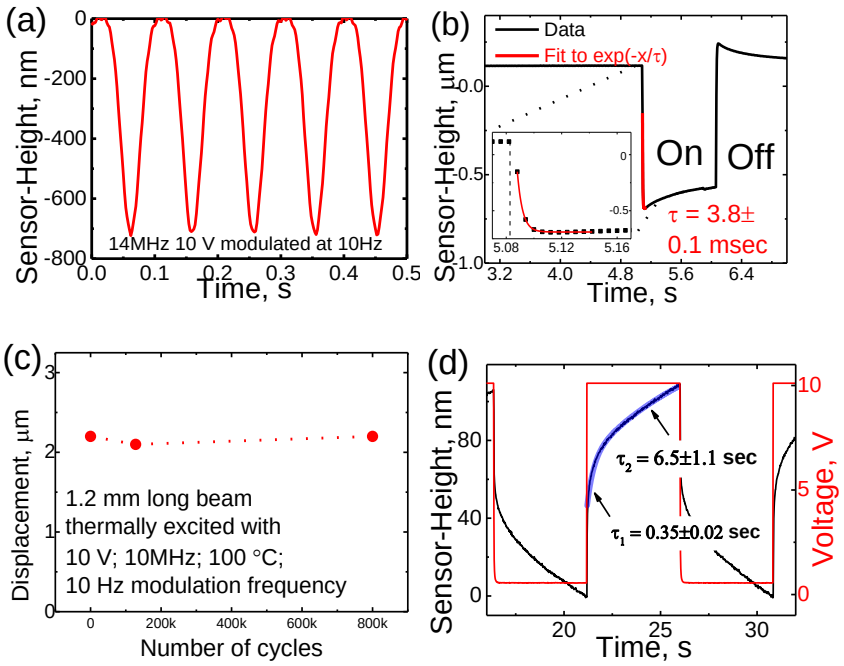

Figure 6. Electro-mechanical effect measured at the center of a 1.2mm beam, in response to an excitation voltage of 10 V at 14 MHz modulated with (a) a sinusoidal amplitude modulation wave of 10 Hz and (b) an On-Off square pulse modulation, using the AFM height-sensor. Inset: Expanded plot showing the region around the On-state onset fitted to an exponential decay function (red curve). (c) Long-term operation measured with the LDV system using the conditions indicated in the panel. (d) AFM time trace measured in response to a square pulse voltage of 10 V with a period of 10 seconds. The response is fitted to an exponential function with two time constants, τ_1 and τ_2, indicated inside the panel.

Acknowledgments

This work was supported in part by the Israeli Ministry of Science and Technology grant #3-12944 and the BioWings project, which has received funding from the European Union's Horizon 2020 under the Future and Emerging Technologies (FET) program with a grant agreement No 801267. This research is made possible in part by the historic generosity of the Harold Perlman Family.

References

[1] N. Setter, *Electroceramic-based MEMS*, Springer, 2005.
[2] M. D. Maeder, D. Damjanovic, N. Setter, J. Electroceram. 2004, 13, 385.
[3] M. Hadad, H. Ashraf, G. Mohanty, C. Sandu, P. Muralt, Acta Mater. 2016, 118, 1.
[4] R. Korobko, A. Patlolla, A. Kossoy, E. Wachtel, H. L. Tuller, A. I. Frenkel, I. Lubomirsky, Adv. Mater. 2012, 24, 5857.
[5] A. Ushakov, E. Mishuk, E. Makagon, D. Alikin, A. Esin, I. Baturin, A. Tselev, V. Y. Shur, I. Lubomirsky, A. Kholkin, Appl. Phys. Lett. 2017, 110, 142902.
[6] A. Kossoy, M. Greenberg, K. Gartsman, I. Lubomirsky, J. Elecrochem. Soc. 2005, 152, C65.
[7] E. Mishuk, E. Makagon, E. Wachtel, S. Cohen, R. Popovitz-Biro, I. Lubomirsky, Sensor Actuat. A-Phys. 2017, 264, 333.
[8] Y. Berg, S. Winter, Z. Kotler, Y. Shacham-Diamand, Journal of Laser Micro/Nanoengineering 2018, 13.
[9] Y. Zhang, Y. Wang, J. Zhang, Y. Liu, X. Yang, Q. Zhang, Ceram. Int. 2015, 41, 6525.
[10] Y. Berg, M. Zenou, O. Dolev, Z. Kotler, Optical Engineering 2015, 54, 011010.
[11] D. Pietroy, Y. Di Maio, B. Moine, E. Baubeau, E. Audouard, Opt Express 2012, 20, 29900.
[12] A. N. Samant, N. B. Dahotre, J. .Europ. Ceram. Soc. 2009, 29, 969.
[13] R. R. Gattass, E. Mazur, Nature photonics 2008, 2, 219.
[14] J.-P. Desbiens, P. Masson, Sensor Actuat. A-Phys. 2007, 136, 554.
[15] N. Uppal, P. S. SHIAKOLAS, S. Priya, Ferroelectric Letters 2005, 32, 67.
[16] A. Ben-Yakar, R. L. Byer, A. Harkin, J. Ashmore, H. A. Stone, M. Shen, E. Mazur, Appl. Phys. Lett. 2003, 83, 3030.
[17] Y. Berg, Z. Kotler, Y. Shacham-Diamand, Journal of Micromechanics and Microengineering 2018, 28, 035009.
[18] C. Hnatovsky, R. Taylor, E. Simova, P. Rajeev, D. Rayner, V. Bhardwaj, P. Corkum, Applied Physics A 2006, 84, 47.
[19] B. N. Chichkov, C. Momma, S. Nolte, F. Von Alvensleben, A. Tünnermann, Applied Physics A 1996, 63, 109.
[20] Y. Di Maio, J.-P. Colombier, P. Cazottes, E. Audouard, Optics and Lasers in Engineering 2012, 50, 1582.
[21] M. C. Gower, Opt Express 2000, 7, 56.
[22] M. Rejab, T. Mon, M. Rashid, N. Shalahim, M. Ismail, International Journal of Recent Trends in Engineering 2009, 1, 105.
[23] A. Benouhiba, D. Belharet, A. Bienaimé, V. Chalvet, M. Rakotondrabe, C. Clévy, Microelectronic Engineering 2018.
[24] B. Pecholt, M. Vendan, Y. Dong, P. Molian, The International Journal of Advanced Manufacturing Technology 2008, 39, 239.
[25] M. C. Gower, "Laser micromachining for manufacturing MEMS devices", presented at *MEMS Components and Applications for Industry, Automobiles, Aerospace, and Communication*, 2001.
[26] S. Hershkovitz, S. Baltianski, Y. Tsur, Sol. State Ionics 2011, 188, 104.
[27] S. Hershkovitz, S. Tomer, S. Baltianski, Y. Tsur, Ecs Transactions 2011, 33, 67.
[28] A. Oz, S. Hershkovitz, N. Belman, E. Tal-Gutelmacher, Y. Tsur, Sol. State Ionics 2016, 288, 311.
[29] A. Oz, D. Gelman, E. Goren, N. Shomrat, S. Baltianski, Y. Tsur, J. Power Sources 2017, 355, 74.
[30] D. Gelman, B. Shvartsev, I. Wallwater, S. Kozokaro, V. Fidelsky, A. Sagy, A. Oz, S. Baltianski, Y. Tsur, Y. Ein-Eli, J. Power Sources 2017, 364, 110.
[31] A. K. Baral, Y. Tsur, Sol. State Ionics 2017, 304, 145.
[32] T. Paul, Y. Tsur, Sol. State Ionics 2018, 323, 37.
[33] S. A. Emam, A. H. Nayfeh, Nonlinear Dynamics 2004, 35, 1.
[34] N. Goykhman, Y. Feldman, E. Wachtel, A. Yoffe, I. Lubomirsky, J. Electroceram. 2014, 33, 180.

[35] A. Kossoy, Y. Feldman, R. Korobko, E. Wachtel, I. Lubomirsky, J. Maier, Adv. Func. Mater. 2009, 19, 634.
[36] A. Kossoy, A. I. Frenkel, Y. Feldman, E. Wachtel, A. Milner, I. Lubomirsky, Sol. State Ionics 2010, 181, 1473.
[37] A. Kossoy, E. Wachtel, I. Lubomirsky, J. Electroceram. 2014, 32, 47.
[38] O. Kraynis, E. Wachtel, I. Lubomirsky, T. Livneh, Scripta Mater. 2017, 137, 123.
[39] E. Wachtel, A. I. Frenkel, I. Lubomirsky, Adv Mater 2018, 30, e1707455.
[40] M. Varenik, S. Cohen, E. Wachtel, A. I. Frenkel, J. C. Nino, I. Lubomirsky, Scripta Mater. 2019, 163, 19.
[41] J.-M. Bae, B. Steele, Sol. State Ionics 1998, 106, 247.
[42] T. Paul, N. Yavo, I. Lubomirsky, Y. Tsur, Sol. State Ionics 2019, 331, 18.
[43] A. Ushakov, E. Mishuk, D. Alikin, B. Slautin, A. Esin, I. Baturin, V. Y. Shur, I. Lubomirsky, A. Kholkin, "Thermal excitation contribution into the electromechanical performance of self-supported Gd-doped ceria membranes", presented at *IOP Conference Series: Materials Science and Engineering*, 2017.
[44] E. Mishuk, A. D. Ushakov, S. R. Cohen, V. Y. Shur, A. L. Kholkin, I. Lubomirsky, Sol. State Ionics 2018, 327, 47.
[45] R. Korobko, A. Lerner, Y. Li, E. Wachtel, A. I. Frenkel, I. Lubomirsky, Appl. Phys. Lett. 2015, 106, 042904.
[46] N. Yavo, O. Yeheskel, E. Wachtel, D. Ehre, A. I. Frenkel, I. Lubomirsky, Acta Mater. 2018, 144, 411.